

Article

Specific Structure and Properties of Composite Membranes Based on the Torlon[®] (Polyamide-imide)/Layered Perovskite Oxide

Alexandra Pulyalina ^{1,*}, Valeriia Rostovtseva ¹, Iana Minich ¹, Oleg Silyukov ¹,
Maria Toikka ¹, Nataliia Saprykina ² and Galina Polotskaya ^{1,2}

¹ Institute of Chemistry, Saint Petersburg State University, Universitetskiy pr. 26, Saint Petersburg 198504, Russia; st017536@student.spbu.ru (V.R.); st048953@student.spbu.ru (I.M.); oleg.silyukov@spbu.ru (O.S.); m.toikka@spbu.ru (M.T.); g_polotskaya@mail.ru (G.P.)

² Institute of Macromolecular Compounds, Russian Academy of Sciences, Bolshoy pr. 31, Saint Petersburg 199004, Russia; elmic@hq.macro.ru

* Correspondence: a.pulyalina@spbu.ru; Tel.: +78-124-284-805

Received: 31 May 2020; Accepted: 1 July 2020; Published: 8 July 2020



Abstract: The use of perovskite-type layered oxide $K_2La_2Ti_3O_{10}$ (Per) as a modifier of the Torlon[®] polyamide-imide (PAI) membrane has led to the formation of a specific structure of a dense nonsymmetrical film, namely, a thin perovskite-enriched layer (3–5 μm) combined with the polymer matrix (~30 μm). The PAI/Per membrane structure was studied by SEM in combination with energy dispersive microanalysis of the elemental composition which illustrated different compositions of top and bottom surfaces of the perovskite-containing membranes. Measurement of water and alcohol contact angles and calculation of surface tension revealed hydrophilization of the membrane surface enriched with perovskite. The transport properties of the nonsymmetrical PAI/Per membranes were studied in the pervaporation of ethanol-ethyl acetate mixture. The inclusion of 2 wt.% Per in the PAI gives a membrane with a high separation factor and increased total flux.

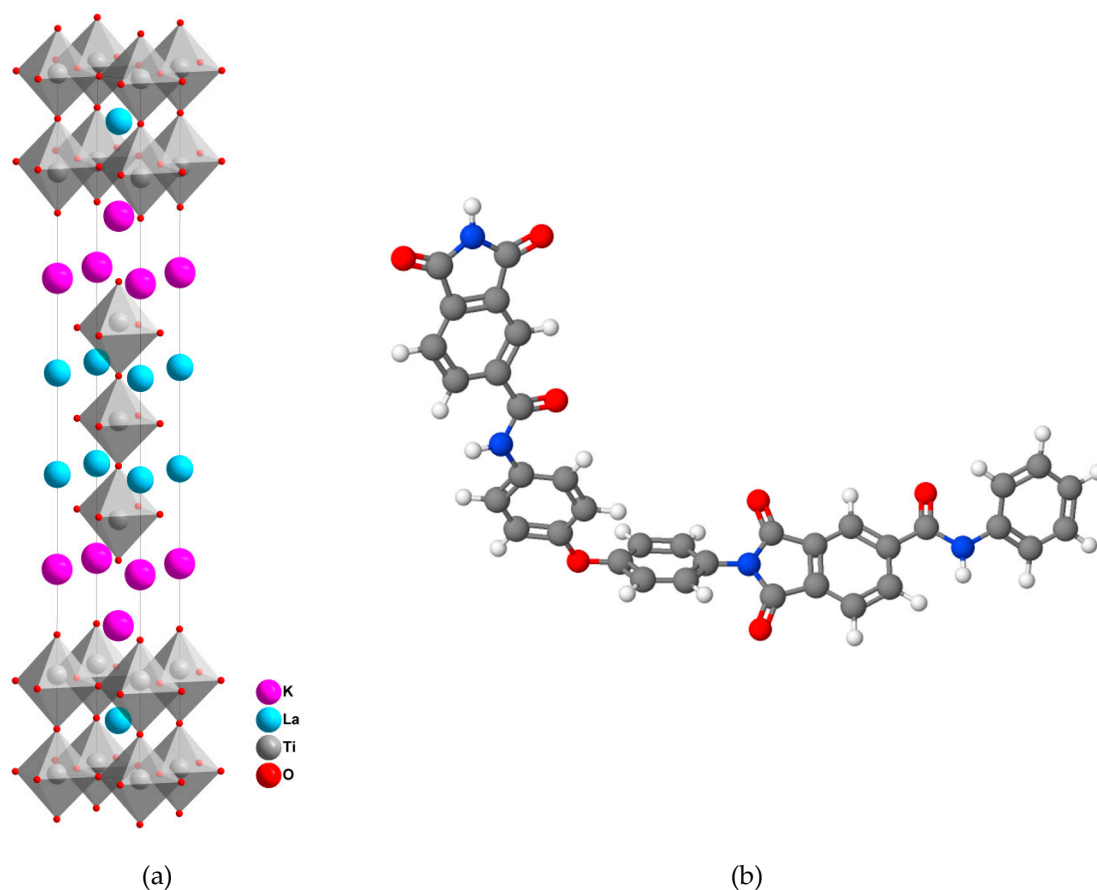
Keywords: perovskite; polyamide-imide; composite membrane; critical surface tension; pervaporation

1. Introduction

Progressive development worldwide depends on technologies that provide energy conservation, as well as minimizing waste and having zero emissions. The concept of an ecological future pushes into the foreground the use of membrane technologies as a favorable substitute for traditional separation processes [1–4].

The key element determining the effectiveness of membrane processes is the membrane. Most processes are carried out at elevated temperatures, therefore the use of membranes based on polymers of a heteroaromatic structure with enhanced thermal and chemical resistance is preferable [5–8]. We chose Torlon[®] polyamide-imide (PAI), a thermoplastic that is characterized by high mechanical strength, a wide temperature range of operation (from $-270\text{ }^\circ\text{C}$ to $+250\text{ }^\circ\text{C}$), chemical resistance, and relative ease of manufacturability. These unique properties cause an interest in the manufacturing membranes based on PAI for ultra- and nanofiltration [9], gas separation [10], and pervaporation [11–16]. However, published works on pervaporation with PAI membranes had aimed alcohol dehydration and data on the performance that were not impressive. To enhance performance, the PAI membranes have been modified by blending with polyesterimide [8], polyimide [9], and gelatin [10]. In the present work, Torlon[®] PAI membrane and its modified form were studied in pervaporation of organic mixture for the first time. We developed a new composite membrane by PAI modification with the perovskite-type layered oxide $K_2La_2Ti_3O_{10}$ (Scheme 1).

Perovskite oxides are mixed metal compounds with a well-defined cubic structure and the general formula ABO_3 , where A and B are various cations, while the B cation is surrounded by an octahedron of O anions [17]. Perovskite-type layered oxide represents solid crystalline species consisting of two-dimensional nanosized plates of perovskite alternating with cations or cationic structural elements. Oxides of this type exhibit ion exchange and intercalation properties including reversible hydration of interlayer space [18,19]. These materials are attractive as components of composites due to the possibility of rearrangement of the metal sections, as well as their stability at elevated temperatures [20–23].



Scheme 1. (a) Crystal structure of perovskite-type layered oxide $K_2La_2Ti_3O_{10}$. (b) Formulas of Torlon[®] polyamide-imide (PAI).

Currently, inorganic membranes based on perovskites are widely used for oxygen purification in catalytic membrane reactors and there are several attempts to use exfoliated perovskite nanosheets as membrane material [24]. However, there is no data on the use of perovskites as modifiers for polymer membranes for pervaporation. Perovskite-type layered oxides seem promising materials for incorporation into membranes due to combination of two factors: (i) the possibility of creating selective transport channels through the interlayer space of the perovskite structure—the presence of ionic compounds in the polymer matrix leads to an increase in the solubility of polar molecules and a decrease in the solubility of nonpolar media, and (ii) the possibility of increasing the distance between polymer chains, which should increase the permeability of the membranes due to the frame of inorganic materials that can prevent the tight packing of polymer chains [25–27].

This work aims to develop a method for manufacturing PAI/Per composites and dense film membranes based on them. The new composite membrane developed in this work is intended for the membrane process of pervaporation, which is used to separate liquid mixtures, including azeotropic, closely boiling, and heat-sensitive liquids [28]. The study on pervaporation separation

of the ethanol–ethyl acetate mixture is of particular interest [29–31] because these liquids have close boiling points (EtOH–78.3 °C, EtOAc–77.0 °C) and form an azeotropic mixture of 26 wt.% ethanol and 74 wt.% ethyl acetate [32]. The impact of perovskites on morphology and physical properties are thoroughly discussed.

2. Materials and Methods

2.1. Materials

PAI Torlon[®] 4000TF, $M_n = 30000$ g/mole, $T_c = 285$ °C, (Solvay Specialty Polymers, Brussel, Belgium) and *N*-methyl pyrrolidone (NMP) were obtained from Aldrich; ethanol (EtOH) and ethyl acetate (EtOAc) were purchased from Vekton (Vekton, Saint Petersburg, Russia). The substances were of chemically pure (CP) grade and used without further purification

2.2. Synthesis of Perovskite

The perovskite $K_2La_2Ti_3O_{10}$ (Per) was synthesized by a hydrothermal method from commercially available precursors. The starting materials were La_2O_3 , 99.9% (Vekton, Saint Petersburg, Russia), TiO_2 P-25 (Evonik, Essen, Germany) and KOH, 99.9% (Vekton, Saint Petersburg, Russia) as both precursor and reaction media. The synthesis was performed in optimized conditions based on the method described earlier [33]. The stoichiometric amounts of TiO_2 and La_2O_3 calculated for 250 mg of the product were weighed and suspended in 40 mL of 4 M KOH. The suspension was sonicated for 15 min and placed in a 50 mL Teflon-lined vessel. The vessel was then inserted into a stainless steel autoclave and heated at 230 °C. After the 72 h reaction period the vessel was naturally cooled in the air for ~3 h and the precipitate was separated by centrifugation. The obtained slurry material was washed once with 40 mL of distilled water and twice with 40 mL of ethanol and dried in air overnight.

As $K_2La_2Ti_3O_{10}$ is known to undergo partial substitution of interlayer potassium cations by protons in water solutions and humid air atmosphere [34], to obtain the stable phase product for membrane preparation the as-synthesized $K_2La_2Ti_3O_{10} \cdot yH_2O$ powder was maintained in distilled water for 24 h forming a partly substituted stable form.

2.3. Perovskite Characterization

The phase compositions characterization was studied by powder XRD-analysis using a Rigaku MiniFlex II diffractometer with Cu $K\alpha$ radiation source in the range of 3–60°, and at a scan speed of 10° min^{-1} . The results of XRD-analysis show the formation of a well-crystallized, single-phase compound after the hydrothermal procedure (see Figure S1).

The morphologies of the obtained samples were carried out by scanning electron microscopy (SEM) (Zeiss Merlin, Oxford Instruments).

2.4. Membrane Preparation

The PAI/Per composites were prepared by mixing solutions of 3 wt.% PAI in NMP and Per in 10 mL of NMP in different amounts to obtain 1–3 wt.% Per in the resulting membranes. The produced solution was sonicated by ultrasound disperser Hielscher UP200St with a 7 mm probe (Hielscher Ultrasonics, Teltow, Germany) for 20 min at 40% amplitude. Then it was coated on a glass plate and left in an oven at 50 °C for a solvent evaporation. In 72 h, membranes were peeled off and placed in a vacuum oven at 60 °C to constant weight. The thicknesses of the resulted membranes were found to be ~33 μm .

2.5. Membrane Characterizations

Membrane morphology was observed using scanning electron microscope SEM Zeiss SUPRA 55VP (Carl Zeiss AG, Oberkochen, Germany). Before the test samples were coated with a platinum 20 nm layer by the Q150R S Plus coater (Quorum Technologies Ltd., Lewes, UK).

The platinum layer of 20 nm thick was coated on the sample surface by cathode sputtering using the Quorum 150 (Great Britain) installation.

Energy dispersive microanalysis (EDS) for study on the elemental composition of samples was performed using a system of microanalysis INCA Energy with an XMax 80 OXFORD detector. Spectra of film surface were examined for phase identification in a sample. Quantitative analysis was performed using the method of fundamental parameters. The standard spectrum accumulation time was 60 s. To determine small amounts of elements, the accumulation time was increased to 300 s.

The contact angle measurements were carried out by a DSA 10-drop shape analyzer (KRÜSS GmbH, Hamburg, Germany) at room temperature and atmospheric pressure using water and n-propanol. Based on measured contact angles, the critical surface tension (σ_s) including dispersion σ_s^d and polar σ_s^p components were calculated by the Owens–Wendt method [35]:

$$\sigma_s = \sigma_s^d + \sigma_s^p \quad (1)$$

Membrane density (ρ) was measured by an immersing a sample (0.05–0.10 g) in chloroform–isopropanol solutions of various compounds in which the membrane remains suspended. Experiments were performed five times with at least two samples.

Fractional free volumes, FFV, of the PAI and composites PAI/Per were calculated by the following equations, respectively [36,37]:

$$FFV = (V_0 - 1.3V_w)/V_0 \quad (2)$$

$$FFV_c = 1 - \rho_c \left(1 - \frac{wt_{Per}\%}{100}\right) \cdot (1 - FFV) \rho_{PAI}^{-1} - \rho_c \rho_{Per} \frac{wt_{Per}\%}{100} \quad (3)$$

where $V_0 = 1/\rho$ is the polymer specific volume and V_w is the van der Waals volume of the PAI macromolecule estimated via Askadskii's group contribution method [38], ρ_{PAI} , ρ_{Per} , and ρ_c are densities of polymer, perovskite, and composites, respectively, and wt_{Per} is the weight fraction of the Per modifier in the polymer matrix.

2.6. Pervaporation

The pervaporation experiment was carried out on a laboratory-scale unit and the details of the apparatus have been described in [39].

The pervaporation results were described in terms of total flux and separation factor. The total flux (J) was determined as the amount of liquid penetrated through membrane area per time interval:

$$J = \frac{Q}{S \cdot t} \quad (4)$$

where Q is the total weight of the permeate collected at time interval t and S is the effective surface area of the membrane.

The separation factor (α) was calculated with the following equation:

$$\alpha = \frac{y/(1-y)}{x/(1-x)} \quad (5)$$

where x and y are the ethanol concentration in the feed and in the permeate, respectively.

3. Results

3.1. Membrane Structure

The morphology of the PAI dense films modified with different amounts of perovskite was studied by scanning electron microscopy (SEM). In Figure 1 micrographs of the cross-section of PAI/Per membranes containing 0, 1, 2, and 3 wt.% Per are presented. The inclusion of perovskite into the PAI changes the film cross-section images—the morphology of the membrane is complicated. Particular

attention is drawn to the film structure inhomogeneous in thickness and a significant difference in morphology near the top and bottom surfaces of the membrane.

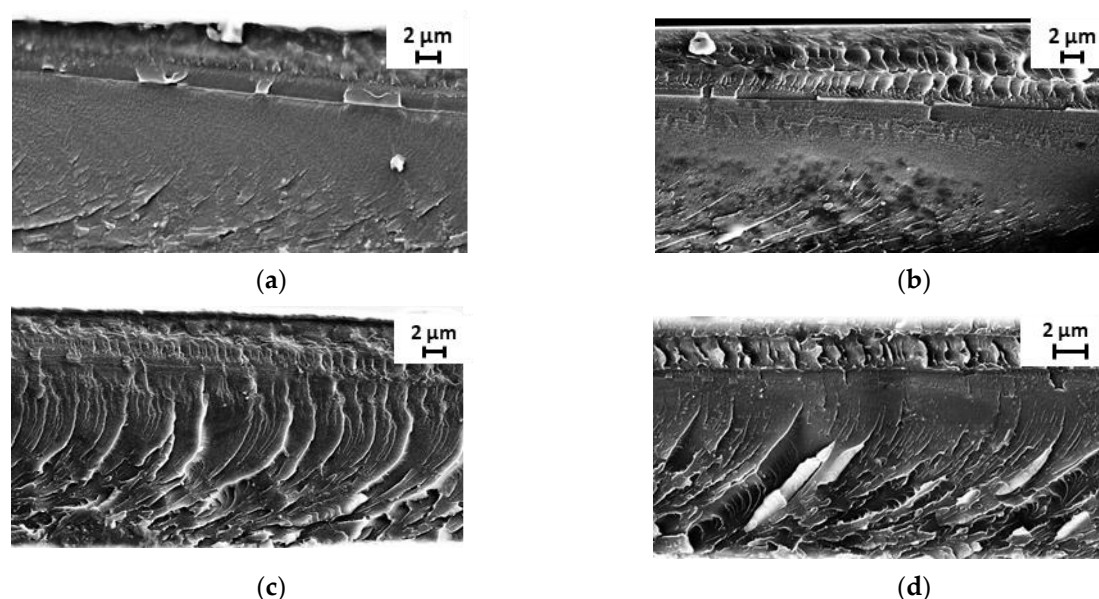


Figure 1. SEM micrographs of membrane cross-section: (a) PAI, (b) PAI/Per (1%), (c) PAI/Per (2%), and (d) PAI/Per (3%). PAI: polyamide-imide; Per: perovskite-type layered oxide $K_2La_2Ti_3O_{10}$.

The top and bottom surfaces of the PAI/Per membranes (Figure 2b–d) differed markedly: a uniform top and a two-component bottom surfaces. The morphology of the top surface of all membranes remains identical while the morphology of the bottom surface changes after modification by perovskites. Figure 2e shows SEM images of as-prepared $K_2La_2Ti_3O_{10}$ oxide particles which have a plate-like morphology typical for layered compounds with lateral sizes of about 2–5 μm and ~4–5 nm thickness. According to Figure 2b–d), the sizes of the perovskite inclusions increase and plate profiles of perovskite inclusions (similar to initial oxide particle morphology) appear.

The elemental composition of the samples was investigated by energy dispersive analysis. It was observed that PAI/Per membranes made of composite materials have different compositions of the top and bottom surfaces. Table 1 shows the data of electron dispersion spectra (EDS) of the elemental analysis of the PAI/Per (2%) membrane along lines (1–5) of the cross-section near the top and bottom surfaces of the membrane. Figure 3 presents a micrograph of the cross-section of the PAI/Per (2%) membrane, where the position of these (1–5) spectral lines is indicated. For all PAI/Per membranes, the EDS of the top surface contains elements (C, N, O) that constitute the chemical formula of PAI. The composition of the bottom surface, in addition to reduced amounts (C, N, O), contains elements K, Ti, and La, which are components of the perovskite. Thus, the data of Table 1 and Figure 3 indicate the nonuniform distribution of perovskite in the PAI matrix along with the depth of the membrane. The spectrum along line 1 (top) does not contain perovskite, which appears in spectrums 3 and 4, and spectrum 5 (bottom) contains the maximum amount of perovskite elements. The filler is concentrated on one side of the membrane, in a layer ~3 μm thick. This may be due to a significant difference in the density of the membrane components: PAI ~1.38 g/cm^3 ; Per ~4.0 g/cm^3 . When preparing the casting solution using an ultrasonic treatment, a uniform transparent PAI/Per (2%) solution is formed. However, after the solution coating to the glass plate, during the evaporation of NMP at 50 $^\circ\text{C}$ for 3–4 h, perovskite diffuses to the bottom under the action of gravity.

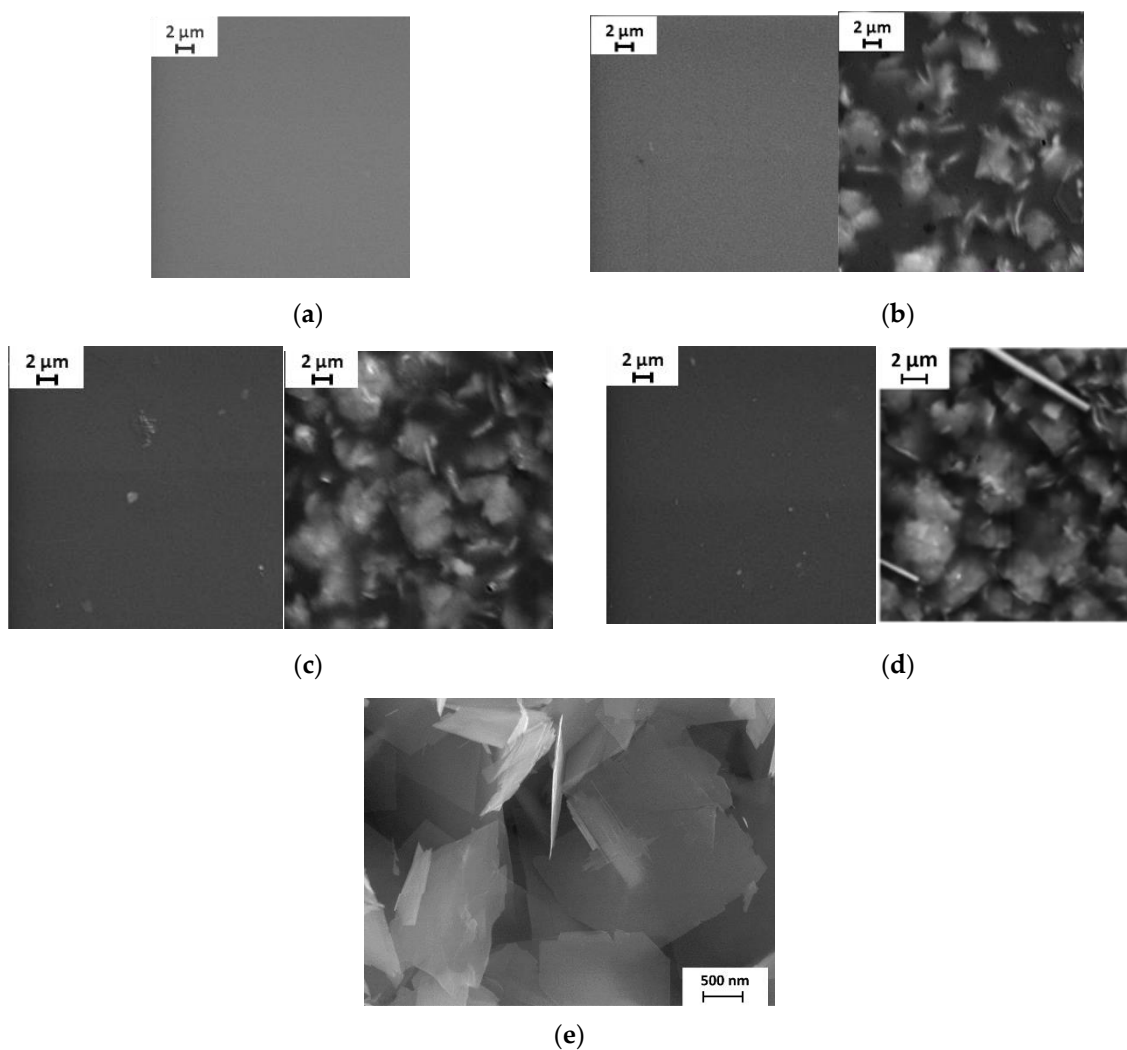


Figure 2. SEM micrographs of the top and bottom surfaces of membranes: (a) PAI, (b) PAI/Per (1%), (c) PAI/Per (2%), (d) PAI/Per (3%), (e) as-prepared $K_2La_2Ti_3O_{10}$ oxide.

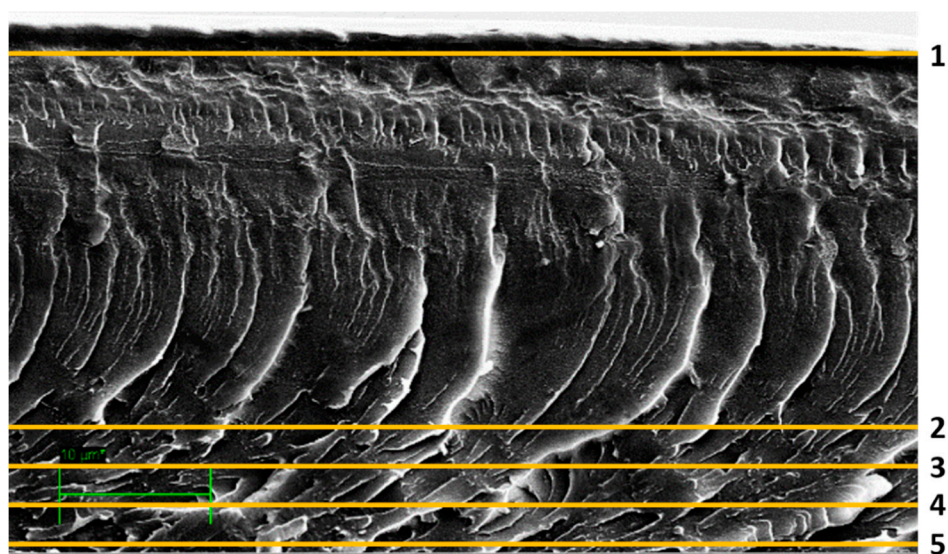


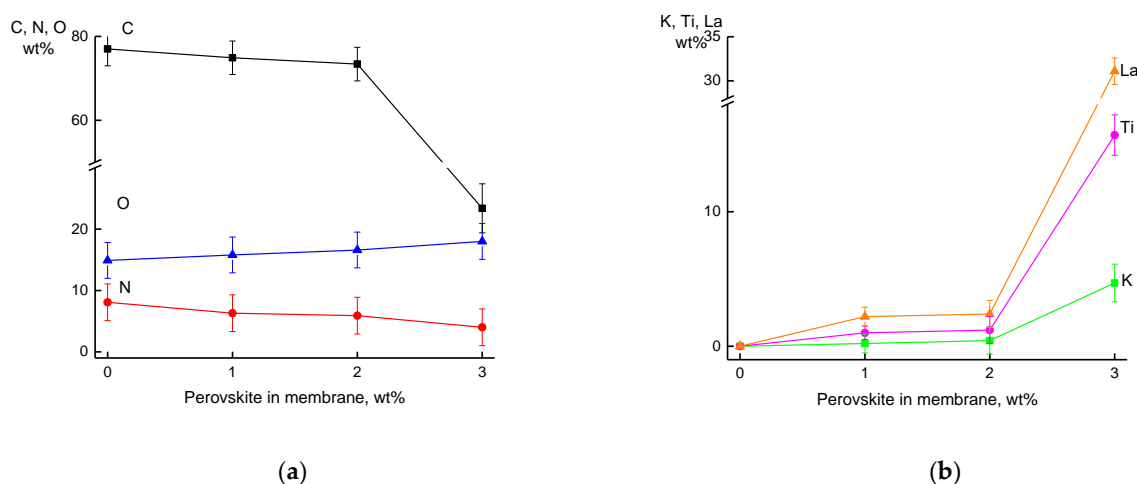
Figure 3. SEM micrographs of PAI/Per (2%) cross-section, where the position of 1–5 spectral lines is indicated.

Table 1. EDS elemental analysis of the cross-section near the top and bottom surfaces of the PAI/Per (2%) membrane.

Spectrum	C wt. %	N wt. %	O wt. %	K wt. %	Ti wt. %	La wt. %	Total wt. %
Spectrum 1 (Top)	77.01	8.08	14.91	0.00	0.00	0.00	100.0
Spectrum 2	75.05	9.06	15.79	0.10	0.00	0.00	100.0
Spectrum 3	74.49	9.07	15.66	0.17	0.00	0.60	100.0
Spectrum 4	77.10	5.85	14.93	0.30	0.73	1.09	100.0
Spectrum 5 (Bottom)	73.39	5.93	16.63	0.42	1.21	2.42	100.0

A similar EDS analysis of the cross-section was carried out for membranes containing also 1 and 3 wt.% perovskite. The same tendency for an increased concentration of perovskite elements was observed on the bottom of all membranes; and in the membrane containing 3 wt.% Per, the concentration of these elements was the highest.

Figure 4 shows the results of the study on surfaces enriched in perovskite for membranes with 0, 1, 2, and 3 wt.% Per. With an increase of the perovskite content in the membrane, the concentration of C and N elements, which are included only in the PAI formula, decreases (Figure 4a); and vice versa, the concentration of K, Ti, and La elements that are components of perovskite increases (Figure 4b). In this case, the concentration of oxygen (O), which is a common element for the both PAI and perovskite, remains unchanged, during decreasing (with the polymer) and increasing (with the filler).

**Figure 4.** Change in the concentration of chemical elements (a) C, N, O, and (b) K, Ti, La on the bottom surface, depending on the perovskite content (0%, 1%, 2%, and 3%) in the PAI/Per membrane.

It was found that PAI/Per membranes have an extraordinary nonsymmetrical structure, unexpected for a manufacturing process such as casting on the plate. The thin perovskite-enriched layer (3–5 μm) is probably bonded by hydrogen and coordination links the polymer component (PAI) of the membrane (~30 μm), as evidenced by the mixed composition of the intermediate layers.

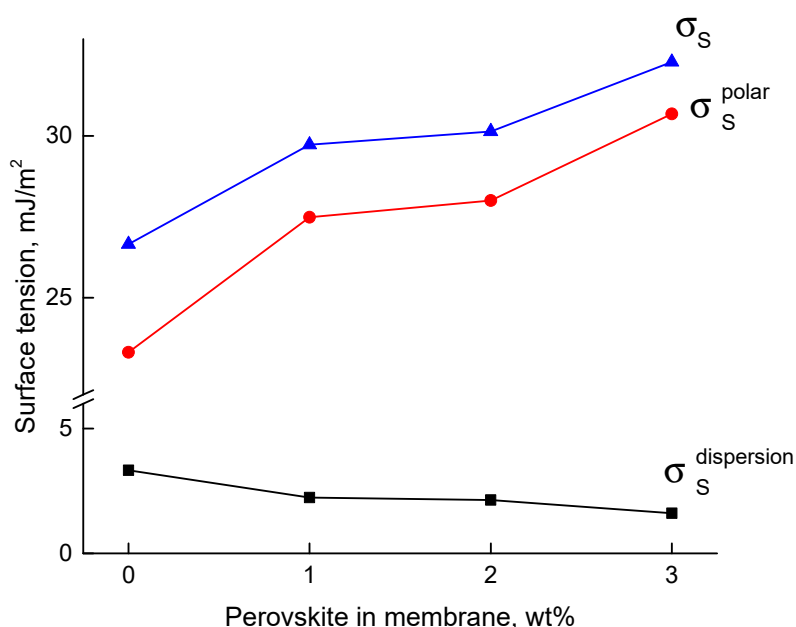
3.2. Surface Tension Properties

The most common characteristic of solid surface tension is the contact angle. Table 2 presents the contact angles of water and *n*-propanol on the surfaces of the PAI/Per membranes containing 0, 1, 2, and 3 wt.% Per. PAI is a rather hydrophilic polymer since the water contact angle on its surface is less than 90°. It should be noted that all measurements were performed on the surface of PAI/Per membranes enriched with perovskite. The inclusion of perovskite reduces the contact angles of water and alcohol for the membranes.

Table 2. Contact angles of PAI/Per membranes.

Membrane	Contact Angle, Degree	
	Water	<i>n</i> -Propanol
PAI	79.4 ± 0.6	14.7 ± 0.3
PAI/Per (1%)	77.1 ± 0.7	13.2 ± 0.2
PAI/Per (2%)	76.8 ± 0.5	12.7 ± 0.2
PAI/Per (3%)	73.4 ± 0.4	11.5 ± 0.1

The data on contact angles were used for calculation of the critical surface tension of PAI/Per membranes. The polar (σ_s^p) and dispersion (σ_s^d) contributions to the critical surface tension (σ_s) were estimated separately. Figure 5 illustrates the dependence of the critical surface tension and its polar and dispersion components on perovskite content in the membrane. As the loading of perovskites was increased, the polar contribution increased but the dispersion contribution decreases. The critical surface tension (σ_s) increases in all cases. Thus, the inclusion of perovskite resulted in a hydrophilization of the composite membrane.

**Figure 5.** Dependence of the surface tension on perovskite content in the membrane.

Fraction free volume (FFV) was calculated based on data from the densities of PAI/Per membranes measured by flotation method. FFV characterizes the elements of the free volume distributed in the polymer matrix. Their presence facilitates the diffusion of molecules of separating mixtures through polymer films and influence on flux in membrane processes. Figure 6 shows FFV values calculated for the PAI/Per films by Equation (3). The FFVs of the composites are higher than that of PAI. This can be referred to a reorganization of polymer chains because of Per incorporation and formation having of not-so-dense macromolecule packaging in the composite membranes as against the PAI membrane. This fact will play a significant role in the study of transport properties of the membranes.

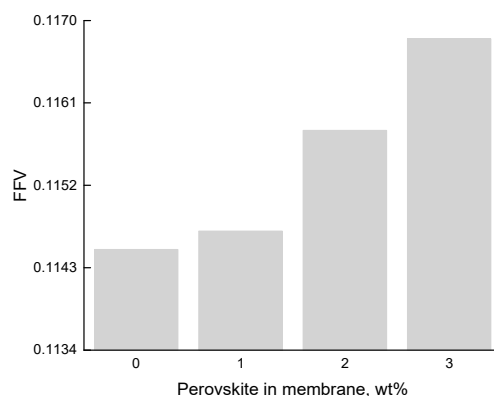


Figure 6. Dependence of fractional free volume (FFV) on perovskite content in membrane.

3.3. Transport Properties

For nonsymmetrical PAI/Per membranes, transport properties were studied in the pervaporation of a two-component ethanol-ethyl acetate mixture. Separation of this mixture may be of independent interest since these liquids form an azeotropic mixture of 26 wt.% ethanol and 74 wt.% ethyl acetate [25].

In addition, this separation task arises during the manufacture of ethyl acetate by esterification (ethanol + acetic acid \leftrightarrow ethyl acetate + water) and the manufacture of butyl acetate by transesterification (ethyl acetate + *n*-butanol \leftrightarrow butyl acetate + ethanol). Considering the peculiarity of the ethyl acetate synthesis, to isolate the target component it is necessary to separate the ethyl acetate from ethanol impurities. In the butyl acetate production, ethanol and ethyl acetate act as by-products and subsequent regeneration of these important organic solvents is required to make them reusable.

Furthermore, the separation of the alcohol-ester system is interesting in view of the assessment of the possibility to shift a chemical equilibrium in the four-component system that occurs during the chemical reaction. This can be done by isolation of the low molecular weight component (alcohol) and thereby increasing the yield of the target product.

Table 3 lists some physical properties of the studied liquids. Ethanol and ethyl acetate have close boiling points and significantly different density, volume, and solubility parameters. Such a characteristic as a solubility parameter, δ , is often used to predict the interaction of a polymer and an organic solvent. In accordance with the solubility theory [40,41], the solubility of a liquid in a polymer is greater, the smaller the difference in their solubility parameters $|\Delta\delta|$. The solubility parameter δ for pure PAI Torlon® is equal to $23.0 \text{ (J/cm}^3\text{)}^{1/2}$. Thus, the solubility of ethanol in the studied membranes should be higher than the solubility of esters.

Table 3. Physical properties of liquids under the study.

Liquid	Mol. Weight, g/mol	Density, g/cm ³	Molar Volume, cm ³ /mol	T _{boiling} , °C	Hildebrand Solubility Parameter, $\delta \text{ (J/cm}^3\text{)}^{1/2}$
Ethanol	46.07	0.789	57.5	78.4	25.9
Ethyl acetate	88.11	0.901	97.8	77.1	18.5

Figure 7 shows the dependences of ethanol concentration in the permeate on ethanol concentration in the feed for the pervaporation of ethanol-ethyl acetate mixture by using PAI and PAI/Per (2%) membranes. The behavior of the permeate concentration versus feed for pervaporation is significantly different from the vapor-liquid equilibrium curve (VLE) for the ethanol-ethyl acetate mixture. In pervaporation, the permeate is enriched with ethanol, and ethanol content in the permeate increases with ethanol concentration in the feed. For each composition of the feed, the position of PAI/Per (2%) membrane is slightly lower than that of the PAI membrane (88 and 86 wt.% ethanol in permeate for PAI and PAI/Per (2%) correspondingly in pervaporation of the azeotropic mixture).

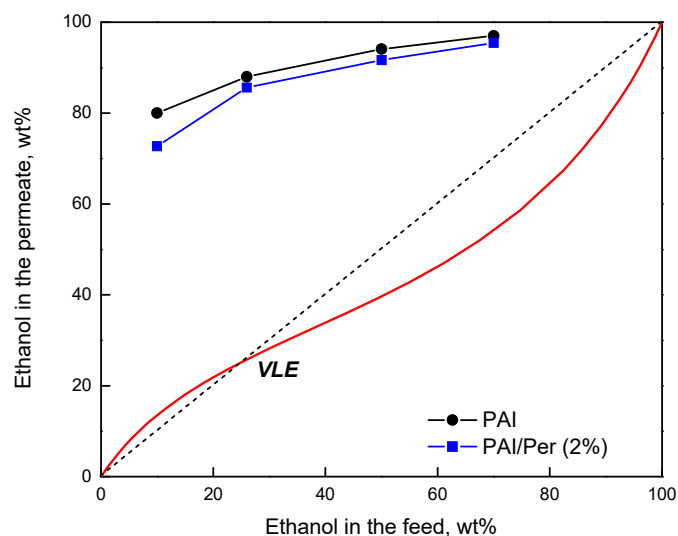


Figure 7. Dependence of ethanol concentration in the permeate on ethanol concentration in the feed for pervaporation using PAI and PAI/Per (2%) membranes; the vapor-liquid equilibrium (VLE) curve for ethanol-ethyl acetate mixture, 40 °C.

Figure 8 demonstrates the main transport properties of PAI and PAI/Per (2%) membranes: total flux and separation factor ($\alpha_{EtOH/EtOAc}$), as well as their dependence on the ethanol concentration in the feed and on the modifier content in the membrane.

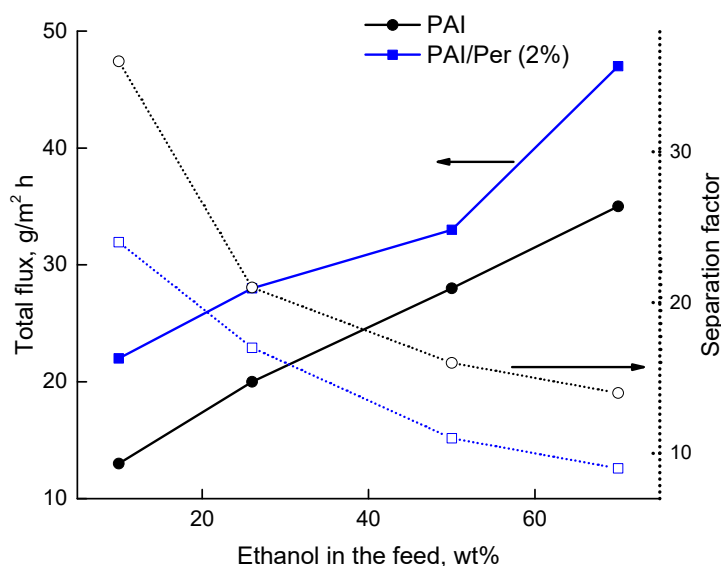


Figure 8. Dependence of the total flux and separation factor ($\alpha_{EtOH/EtOAc}$) on the ethanol concentration in the feed for pervaporation of the ethanol-ethyl acetate mixture using PAI and PAI/Per (2%) membranes, 40 °C.

From the data in Figure 8 it follows that the total flux of the membranes increases with the growth of ethanol concentration in the feed, while the flux is higher up to 1.5 times for PAI/Per (2%) membrane as compared with the unmodified PAI membrane. An opposite relationship was obtained for the separation factor ($\alpha_{EtOH/EtOAc}$) which decreases with the growth of ethanol concentration in the feed. According to $\alpha_{EtOH/EtOAc}$ calculated using data on component concentrations in the feed and permeate, the selectivity of the membrane containing 2% Per is slightly lower compared with the unmodified PAI membrane.

Transport properties of membranes developed in this work were compared with literature data (not numerous) for the pervaporation of the ethanol-ethyl acetate mixture. Table 4 lists data on total flux and separation factors that have been obtained by the use of different membranes [23,24,34]. It should be noted that No 3 is nonpolymeric membranes [24]. Membranes from polydimethylsiloxane (PDMS) exhibit high total flux and a small separation factor [30]. The separation of ethanol-ethyl acetate mixture is a difficult task. According to Table 4, separation factors of known membranes are equal to (1.1–3.25) however the results of our work are superior to these data. The separation factor of the ethanol-ethyl acetate mixture, even of the azeotropic composition, is very high for the PAI and PAI/Per (2%) membranes and equal to 21 and 17, respectively. The total flux is higher for PAI/Per (2%) as compared with the unmodified PAI membrane.

Table 4. Comparison of transport properties of the present membranes with literature data on pervaporation of the ethanol-ethyl acetate azeotropic mixture. PDMS: Polydimethylsiloxane.

No	Membrane	Ethanol in the Feed, wt. %	Total Flux, g/m ² h	Separation Factor	Ref.
1	PDMS	20	4884	1.5	[30]
2	BP-SILM-70	30	70	3	[31]
3	PEBAX	60		1.1	[42]
4	PDMS	60		3.25	[42]
5	PERVAP 4060	60		2	[42]
6	PAI	26	20	21	Present work
7	PAI/Per(2%)	26	28	17	Present work

PDMS – polydimethylsiloxane; BP-SILM-70 – buckypaper supported ionic liquid membrane; PEBAX – polyether block amide; PERVAP 4060 – commercial composite membrane based on polysiloxane.

4. Conclusions

A method for producing novel composite membranes by inclusion of up to 3 wt.% perovskite-type layered oxide $K_2La_2Ti_3O_{10}$ into the Torlon[®] PAI matrix was developed. This method consists of mixing solutions of these components in NMP, sonication, casting on a glass plate, followed by evaporation of the solvent.

The membrane structure was studied by SEM in combination with energy dispersive analysis of the elemental composition. It was found that PAI/Per membranes have an extraordinary nonsymmetrical structure, unexpected for a manufacturing process such as casting on the plate; and a thin perovskite-enriched layer (3–5 μm) combined with the polymer component of the membrane (PAI) (~30 μm).

The creation of a layer containing perovskite in the composite membrane leads to hydrophilization of the membrane surface, as evidenced by a decrease in the contact angles for water and alcohol with an increase in the perovskite content in the membrane.

The transport properties of the nonsymmetrical PAI/Per membrane were studied during the pervaporation of ethanol-ethyl acetate mixture and compared with literature data. It was found that PAI/Per 2% membrane has a high separation factor, mainly removing ethanol, even from a mixture of azeotropic composition. The inclusion of perovskite in the Torlon[®] PAI membrane leads to an increase of the total flux.

Supplementary Materials: The following are available online at <http://www.mdpi.com/2073-8994/12/7/1142/s1>, Figure S1: XRD patterns for as-prepared $K_2La_2Ti_3O_{10}$ (KLT₃) and the product after 24 h water treatment HKLT₃.

Author Contributions: Membrane preparation, physicochemical investigations, analysis of transport properties in pervaporation were carried out by V.R., A.P., and G.P. Synthesis and investigation of perovskites was conducted by I.M. and O.S. N.S. held SEM and EDS analysis of the membranes. Writing—review & editing, A.P., V.R., I.M., O.S., M.T., N.S. and G.P. All authors have read and agreed to the published version of the manuscript.

Funding: Membrane formation, investigation of structure and transport properties of the membranes were funded by the Russian Science Foundation (RSF) [grant 18-79-10116]. M.T., A.P., and V.R. also thank the Russian Foundation for Basic Research [grant 18-33-20138] for financial support of studies of the physical parameters and vapor-liquid equilibrium of separating liquids. Layered perovskite oxide was synthesized under grant [18-03-00915] of Russian Foundation for Basic Research. V.R. thanks the Russian Foundation for Basic Research [grant 19-33-90048] for financial support of layered perovskite oxide-polymers composites formation studies.

Conflicts of Interest: The authors declare no conflict of interest.

References

1. Baker, R.W. *Membrane Technology and Applications*, 3rd ed.; Wiley: Chichester, UK, 2012; ISBN 9780470743720.
2. Genduso, G.; Luis, P.; Van der Bruggen, B. Pervaporation membrane reactors (PVMRs) for esterification. In *Membrane Reactors for Energy Applications and Basic Chemical Production*; Elsevier Inc.: Amsterdam, The Netherlands, 2015; pp. 565–603. ISBN 9781782422273.
3. Buonomenna, M.G. Design Next Generation Membranes or Rethink the “Old” Asymmetric Membranes? *Symmetry (Basel)* **2020**, *12*, 270. [[CrossRef](#)]
4. Buonomenna, M.G. Energy Storage and Conversion Technologies: The Nanotechnology Role in their Advances. *Recent Pat. Nanotechnol.* **2017**, *11*. [[CrossRef](#)] [[PubMed](#)]
5. Pulyalina, A.Y.; Polotskaya, G.A.; Toikka, A.M. Membrane materials based on polyheteroarylenes and their application for pervaporation. *Russ. Chem. Rev.* **2016**, *85*. [[CrossRef](#)]
6. Kreiter, R.; Wolfs, D.; Engelen, C.; Vanveen, H.; Vente, J. High-temperature pervaporation performance of ceramic-supported polyimide membranes in the dehydration of alcohols. *J. Memb. Sci.* **2008**, *319*, 126–132. [[CrossRef](#)]
7. Pulyalina, A.Y.; Toikka, A.M.; Polotskaya, G.A. Investigation of pervaporation membranes based on polycarbamide: Effect of residual solvent. *Pet. Chem.* **2014**, *54*, 573–579. [[CrossRef](#)]
8. Pulyalina, A.Y.; Polotskaya, G.A.; Kalyuzhnaya, L.M.; Sushchenko, I.G.; Meleshko, T.K.; Yakimanskii, A.V.; Chislov, M.V.; Toikka, A.M. Sorption and transport of aqueous isopropanol solutions in polyimide-poly(aniline-co-anthranilic acid) composites. *Russ. J. Appl. Chem.* **2011**, *84*, 840–846. [[CrossRef](#)]
9. Sun, S.P.; Wang, K.Y.; Peng, N.; Hatton, T.A.; Chung, T.S. Novel polyamide-imide/cellulose acetate dual-layer hollow fiber membranes for nanofiltration. *J. Memb. Sci.* **2010**, *363*, 232–242. [[CrossRef](#)]
10. Peng, N.; Chung, T.S. The effects of spinneret dimension and hollow fiber dimension on gas separation performance of ultra-thin defect-free Torlon[®] hollow fiber membranes. *J. Memb. Sci.* **2008**, *310*, 455–465. [[CrossRef](#)]
11. Wang, Y.; Jiang, L.; Matsuura, T.; Chung, T.S.; Goh, S.H. Investigation of the fundamental differences between polyamide-imide (PAI) and polyetherimide (PEI) membranes for isopropanol dehydration via pervaporation. *J. Memb. Sci.* **2008**, *318*, 217–226. [[CrossRef](#)]
12. Wang, Y.; Goh, S.H.; Chung, T.S.; Na, P. Polyamide-imide/polyetherimide dual-layer hollow fiber membranes for pervaporation dehydration of C1-C4 alcohols. *J. Memb. Sci.* **2009**, *326*, 222–233. [[CrossRef](#)]
13. Teoh, M.M.; Chung, T.S.; Wang, K.Y.; Guiver, M.D. Exploring Torlon/P84 co-polyamide-imide blended hollow fibers and their chemical cross-linking modifications for pervaporation dehydration of isopropanol. *Sep. Purif. Technol.* **2008**, *61*, 404–413. [[CrossRef](#)]
14. Yoshikawa, M.; Higuchi, A.; Ishikawa, M.; Guiver, M.D.; Robertson, G.P. Vapor permeation of aqueous 2-propanol solutions through gelatin/Torlon[®] poly(amide imide) blended membranes. *J. Memb. Sci.* **2004**, *243*, 89–95. [[CrossRef](#)]
15. Higuchi, A.; Yoshikawa, M.; Guiver, M.D.; Robertson, G.P. Vapor permeation and pervaporation of aqueous 2-propanol solutions through the Torlon[®] poly(amide imide) membrane. *Sep. Sci. Technol.* **2005**, *40*, 2697–2707. [[CrossRef](#)]
16. Adoor, S.G.; Manjeshwar, L.S.; Bhat, S.D.; Aminabhavi, T.M. Aluminum-rich zeolite beta incorporated sodium alginate mixed matrix membranes for pervaporation dehydration and esterification of ethanol and acetic acid. *J. Memb. Sci.* **2008**, *318*, 233–246. [[CrossRef](#)]
17. Nair, S.P.N.; Murugavel, P. Oxides: Their Properties and Uses. In *Comprehensive Inorganic Chemistry II (Second Edition): From Elements to Applications*; Elsevier Ltd.: Amsterdam, The Netherlands, 2013; Volume 4, pp. 47–72. ISBN 9780080965291.

18. Uppuluri, R.; Sen Gupta, A.; Rosas, A.S.; Mallouk, T.E. Soft chemistry of ion-exchangeable layered metal oxides. *Chem. Soc. Rev.* **2018**, *47*, 2401–2430. [[CrossRef](#)]
19. Schaak, R.E.; Mallouk, T.E. Perovskites by design: A toolbox of solid-state reactions. *Chem. Mater.* **2002**, *14*, 1455–1471. [[CrossRef](#)]
20. Vente, J.F.; Haije, W.G.; Rak, Z.S. Performance of functional perovskite membranes for oxygen production. *J. Memb. Sci.* **2006**, *276*, 178–184. [[CrossRef](#)]
21. Song, Z.; Zhang, Z.; Zhang, G.; Liu, Z.; Zhu, J.; Jin, W. Effects of polymer binders on separation performance of the perovskite-type 4-bore hollow fiber membranes. *Sep. Purif. Technol.* **2017**, *187*, 294–302. [[CrossRef](#)]
22. Guironnet, L.; Geffroy, P.M.; Tessier-Doyen, N.; Boulle, A.; Richet, N.; Chartier, T. The surface roughness effect on electrochemical properties of La_{0.5}Sr_{0.5}Fe_{0.7}Ga_{0.3}O_{3-Δ} perovskite for oxygen transport membranes. *J. Memb. Sci.* **2019**, *588*, 117199. [[CrossRef](#)]
23. Prajontat, P.; Sriprachuabwong, C.; Wongkanya, R.; Dechtrirat, D.; Sudchanham, J.; Srisamran, N.; Sangthong, W.; Chuysinuan, P.; Tuantranont, A.; Hannongbua, S.; et al. Moisture-Resistant Electrospun Polymer Membranes for Efficient and Stable Fully Printable Perovskite Solar Cells Prepared in Humid Air. *ACS Appl. Mater. Interfaces* **2019**, *11*, 27677–27685. [[CrossRef](#)]
24. Nakagawa, K.; Yamashita, H.; Saeki, D.; Yoshioka, T.; Shintani, T.; Kamio, E.; Kreissl, H.T.; Tsang, S.C.E.; Sugiyama, S.; Matsuyama, H. Niobate nanosheet membranes with enhanced stability for nanofiltration. *Chem. Commun.* **2017**, *53*, 7929–7932. [[CrossRef](#)] [[PubMed](#)]
25. Avagimova, N.V.; Pulyalina, A.Y.; Toikka, A.M.; Suvorova, O.M.; Vilesov, A.D.; Polotskaya, G.A. Controlling the barrier properties of polymer composites containing montmorillonite. *Pet. Chem.* **2013**, *53*, 559–563. [[CrossRef](#)]
26. Gao, C.; Zhang, M.; Jiang, Z.; Liao, J.; Xie, X.; Huang, T.; Zhao, J.; Bai, J.; Pan, F. Preparation of a highly water-selective membrane for dehydration of acetone by incorporating potassium montmorillonite to construct ionized water channel. *Chem. Eng. Sci.* **2015**, *135*, 461–471. [[CrossRef](#)]
27. Choudhari, S.K.; Kariduraganavar, M.Y. Development of novel composite membranes using quaternized chitosan and Na⁺-MMT clay for the pervaporation dehydration of isopropanol. *J. Colloid Interface Sci.* **2009**, *338*, 111–120. [[CrossRef](#)]
28. Roy, S.; Singha, N. Polymeric Nanocomposite Membranes for Next Generation Pervaporation Process: Strategies, Challenges and Future Prospects. *Membranes (Basel)* **2017**, *7*, 53. [[CrossRef](#)] [[PubMed](#)]
29. Sato, K.; Sugimoto, K.; Nakane, T. Separation of ethanol/ethyl acetate mixture by pervaporation at 100–130 °C through NaY zeolite membrane for industrial purpose. *Microporous Mesoporous Mater.* **2008**, *115*, 170–175. [[CrossRef](#)]
30. Hasanoğlu, A.; Salt, Y.; Keleşer, S.; Özkan, S.; Dinçer, S. Pervaporation separation of ethyl acetate-ethanol binary mixtures using polydimethylsiloxane membranes. *Chem. Eng. Process. Process Intensif.* **2005**, *44*, 375–381. [[CrossRef](#)]
31. Ong, Y.T.; Tan, S.H. Pervaporation separation of a ternary azeotrope containing ethyl acetate, ethanol and water using a buckypaper supported ionic liquid membrane. *Chem. Eng. Res. Des.* **2016**, *109*, 116–126. [[CrossRef](#)]
32. PD. CRC Handbook of Chemistry and Physics. *J. Mol. Struct.* **1992**, *268*, 320. [[CrossRef](#)]
33. Huang, Y.; Wu, J.; Wei, Y.; Lin, J.; Huang, M. Hydrothermal synthesis of K₂La₂Ti₃O₁₀ and photocatalytic splitting of water. *J. Alloys Compd.* **2008**, *456*, 364–367. [[CrossRef](#)]
34. Rodionov, I.A.; Mechtaeva, E.V.; Burovikhina, A.A.; Silyukov, O.I.; Toikka, M.A.; Zvereva, I.A. Effect of protonation on the photocatalytic activity of the K₂La₂Ti₃O₁₀ layered oxide in the reaction of hydrogen production. *Monatshefte für Chemie-Chem. Mon.* **2018**, *149*, 475–482. [[CrossRef](#)]
35. Owens, D.K.; Wendt, R.C. Estimation of the surface free energy of polymers. *J. Appl. Polym. Sci.* **1969**, *13*, 1741–1747. [[CrossRef](#)]
36. Boyer, R.F. Physical properties of molecular crystals, liquids and glasses. *J. Polym. Sci. Part A-1 Polym. Chem.* **1969**, *7*, 2466. [[CrossRef](#)]
37. Zhang, H.; Wang, S.; Weber, S.G. Morphology and free volume of nanocomposite Teflon AF 2400 films and their relationship to transport behavior. *J. Memb. Sci.* **2013**, *443*, 115–123. [[CrossRef](#)]
38. Askadskii, A.A. *Computational Materials Science of Polymers*; Cambridge International Science Publishing Conditions: Cambridge, UK, 2003; ISBN 1898326622.

39. Pulyalina, A.; Tataurov, M.; Faykov, I.; Rostovtseva, V.; Polotskaya, G. Polyimide Asymmetric Membrane vs. Dense Film for Purification of MTBE Oxygenate by Pervaporation. *Symmetry (Basel)* **2020**, *12*, 436. [[CrossRef](#)]
40. Belmares, M.; Blanco, M.; Goddard, W.A.; Ross, R.B.; Caldwell, G.; Chou, S.H.; Pham, J.; Olofson, P.M.; Thomas, C. Hildebrand and hansen solubility parameters from molecular dynamics with applications to electronic nose polymer sensors. *J. Comput. Chem.* **2004**, *25*, 1814–1826. [[CrossRef](#)] [[PubMed](#)]
41. Barton, A.F.M. *CRC Handbook of Solubility Parameters and Other Cohesion Parameters*; CRC Press: Boca Raton, FL, USA, 1991; ISBN 9780849301766.
42. Knozowska, K.; Li, G.; Kujawski, W.; Kujawa, J. Novel heterogeneous membranes for enhanced separation in organic-organic pervaporation. *J. Memb. Sci.* **2020**, *599*, 117814. [[CrossRef](#)]



© 2020 by the authors. Licensee MDPI, Basel, Switzerland. This article is an open access article distributed under the terms and conditions of the Creative Commons Attribution (CC BY) license (<http://creativecommons.org/licenses/by/4.0/>).